



DeepCwind semi-submersible floating offshore wind turbine platform with a nonlinear multi-segment catenary mooring line and intermediate buoy

Mohammad Motallebi¹, Hassan Ghassemi², Mehdi Shokouhian³

¹  <https://orcid.org/0000-0003-2843-1737>


²  <https://orcid.org/0000-0002-6201-346X>

³  <https://orcid.org/0000-0001-9823-0661>

^{1,2} Amirkabir University of Technology, Tehran, Iran

¹ Department of Civil and Environmental Engineering, ² Department of Maritime Engineering
e-mail: ¹ m_motallebi@aut.ac.ir, ² gasemi@aut.ac.ir

³ Morgan State University, Department of Civil Engineering, Baltimore, USA
e-mail: Mehdi.shokouhian@morgan.edu

 corresponding author

Keywords: semi-submersible floating platform, offshore wind turbine, dynamic response, catenary mooring system, intermediate buoy, strain and tension

JEL Classification: C02, C32, C61, C63, L61, Q01, Q56

Abstract

In this paper, to improve the mechanical behavior of DeepCwind semi-submersible floating offshore wind turbine (FOWT) platform mooring lines, the nonlinear catenary cables of the platform were divided into multi-segment and intermediate buoys. Mathematical formulations of the boundary element method (BEM) governing the dynamics of mooring line systems with buoy devices were described. This study was applied to the OC4-DeepCwind semi-submersible FOWT platform, which is designed for a 200-meter water depth with mooring lines consisting of three catenary steel chain cables at 120° angles to each other. The dynamic response of the multi-segment catenary mooring lines with different buoy radiuses and different positions along the cables was investigated. The full-scale platform was modeled in ANSYS-AQWA software, and the simulations were performed under harsh offshore conditions. The mooring line's general arrangement, tension, strain and uplift force for different buoy radiuses and their position along the cable are presented and discussed. Moreover, platform motions in three directions (surge, heave, and pitch) were also analyzed. It was concluded that by correctly selecting the buoy volume and position along the cable, the tension of the cable may be reduced by up to 45%. By incorrectly selecting the buoy, the results caused adverse effects.

Introduction

Semi-submersible floating platforms are one of the most common deep-water sub-structures for FOWTs. Mooring of floating units is one of the most important parts of the design and erection of these floating platforms in deep water. According to Bae's investigations, failure of one cable of an OC4-DeepCwind semi-submersible FOWT's mooring line can

result in over 700 m drift, which can damage other structures in offshore wind farms (Bae, Kim & Kim, 2016). In a semi-submersible drilling platform, to ensure safe operation and prevent damage to excavation equipment, the horizontal movements of the platform should be limited to less than 1% of the water depth, where the major restriction of horizontal responses is provided by mooring lines (Sabziyan et al., 2014). Full-scale fatigue assessment testing of

catenary steel chain mooring under tensile loads was performed by Martinez Perez et al. (Martinez Perez et al., 2019) under similar saline water conditions. The purpose was to predict the fatigue lifetime and identify the locations of fatigue failure in the chains. It has been found that chain failure often occurs at the point of the intrados (KT point) and crown zones because of localized stress concentration in these areas. Hence, investigations of the resulting forces and the mechanical behavior of mooring lines of semi-submersible floating wind turbine platforms to derive safe conditions and prevent potential risks have always been a major concern. Hall and Goupee (Hall & Goupee, 2015) simulated a DeepCwind semi-submersible FOWT system, including its mooring dynamics. They introduced a lumped-mass mooring line model and validated it against experimental data from a scale-model floating offshore wind turbine. Azcona et al. (Azcona et al., 2016) developed a code for the dynamic response of mooring lines based on the finite-element method, with three translational degrees of freedom in each node of lumped mass. A new frequency-domain modeling approach was presented for FOWTs with a coupled wind turbine, floating platform, and mooring system sub-models. The sub-models were generated using the validated numerical tools Fast and Wamit to obtain the frequency domain aerodynamic and hydrodynamic characteristics, respectively, for any given design candidate (Karimi, Buckham & Crawford, 2019). The low-frequency drift effect should be considered when TLP loses tendons. The in-plane second-order hydrodynamic loads reached approximately 10%, to a maximum of 40% of total horizontal loads. This phenomenon magnified the TLP's horizontal offset and rotation (Yu et al., 2019). Lee et al. (Lee, Han & Park, 2015) explored the causes of the mooring system's failure for a typical marine vessel. Then, using the results of dynamic and static analyses, an equation to predict exert tension of mooring lines was presented. They increased the safety factor against fairlead mooring failure by using a bitt foundation plate and bolts at the fairlead point.

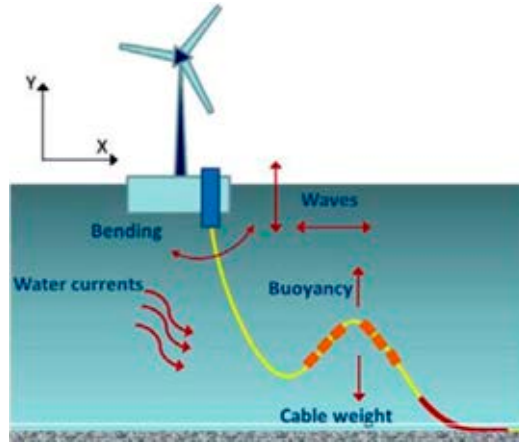
Since the semi-submersible DeepCwind platform mooring line system consists of steel chains (Robertson et al., 2014), the benefits of this system versus other materials such as wire or synthetic ropes, include easy installation, convenient repair, lower installation cost, high resistance against abrasion or marine growth, and high stability against offset due to high deadweight. On the other hand, the disadvantages of this mooring system include low elasticity and intermediate fatigue resistance. Also,

as the water depth increases, the weight of chains becomes too large, and the vertical forces due to the weight of the cables, which apply to the float, will increase. Consequently, due to the increase in weight, costs also increase, making the system economically infeasible, although it increases the capacity of the system against exerting forces. The benefits of using a buoy in deep-water catenary mooring systems include lighter chains and mooring system wires, a reduction in the pre-tension and element strain along the cable, as well as a reduction in the cable's weight and radius of containment, which lowers construction costs and enhances operational safety. There are advantages and disadvantages of applying buoys in catenary mooring lines, including a reduction in the weight of heavy chains and wires and less pre-tension. This also diminishes the mooring radius and decreases the influence of other cable installations. The third advantage is the presence of the restoring force and the ability to resist harsher ocean loads. The disadvantages of applying buoys in catenary mooring lines are a longer installation process, the risk of buoy damage, and more complex dynamic characteristics of the hybrid mooring line. Figure 1 shows the semi-submersible FOWT platform and mooring line system.

The idea of using buoys in the mooring line systems has attracted the attention of researchers. Static analysis of the chain cables with buoys was investigated by Wang (Wang, 2007) to determine the effect of the buoy's size and the weight of the buoy on cables' tension. Qiao et al. (Qiao, Yan & Ou, 2014) studied the effect of buoys on the dynamics of mooring systems and the motion response of a platform. Ghaffari and Dardel (Ghaffari & Dardel, 2018) examined the effect of diameter and number of buoys on the response of the Amirkabir semi-submersible drilling platform. The results showed that upon increasing the number of buoys, the time domain response amplitude of surge motion was reduced, while under heave and pitch motions, the oscillation amplitude was increased. Kwan and Bruen (Kwan & Bruen, 1991) compared dynamic calculation methods, including the frequency domain, the time domain, and the quasi-static methods using numerical simulations. They recommended using the time domain method for nonlinear dynamic analyses of cables with buoys. The attached buoys could reduce the tension on the mooring lines. This was a significant improvement for the mooring system since it provided a good approach to solve the trade-off between the vessel's motion and the lines' tension (Yuan, Incecik & Ji, 2014).



OC4-DeepCwind semi-submersible FOWT platform



Semi-submersible FOWT and mooring line



Spherical buoy

Figure 1. Semi-submersible FOWT platform with mooring line and buoy

For this reason, this paper investigates the influence of buoys with different dimensions and their positions to obtain the appropriate configuration to decrease the tension, element strain, and to uplift the mooring lines without noticeably altering the DeepCwind FOWT motions in harsh offshore environments. In this regard, the ANSYS-AQWA solver was used to analyze the mooring lines by discretizing them into nonlinear stiffness springs (nonlinear stress-strain springs). In this vein, van den Boom (van den Boom, 1985) showed that the tension resonance dynamics were strongly influenced by nonlinearities due to catenary effects such as large transverse displacements at the midpoint of mooring lines and the elasticity and drag coefficient; thus, this would not be considered in frequency domain models. Brown and Mavrakos (Brown & Mavrakos, 1999) studied various systems of mooring lines and revealed that by using nonlinear time-domain methods, the mooring line tension and damping results were generally in good agreement. In contrast, the results of the frequency-domain analysis showed large scattering and significant disagreements compared with nonlinear time-domain methods, especially the damping coefficients.

Mathematical formulations

Dynamic of catenary mooring line

To analyze the dynamics of the cable motion, many factors must be considered, such as the effects of cable mass, drag forces, inline elastic tension, and bending moment. The forces applied to the cable vary with time, and the cables generally behave nonlinearly. A simulation of cable dynamics is needed

to discretize the cable along its length and assemble the mass and applied forces. Each mooring line should be discretized in a spring-mass chain of N Morison-type elements (Dessi, Carcaterra & Diotati, 2004) subjected to various external forces, as shown in Figure 2. The general equations for the force and moment acted to the mooring line cable are expressed as follows:

$$\frac{\partial \vec{T}}{\partial S_e} + \frac{\partial \vec{V}}{\partial S_e} + \vec{w} + \vec{F}_h = m \frac{\partial^2 \vec{R}}{\partial t^2} \quad (1)$$

$$\frac{\partial \vec{M}}{\partial S_e} + \frac{\partial \vec{R}}{\partial S_e} \times \vec{V} = -\vec{q}$$

where m is the mass of the cable element per unit length; \vec{q} , \vec{V} , \vec{M} , \vec{T} , \vec{R} are distributed moment (which is assumed to be zero), shear force, bending moment, tension force, and position vectors of the first node from the cable element, respectively; S_e is the partial length of the element; \vec{F}_h and \vec{w} are the external hydrodynamic forces and weight vectors per unit length, respectively.

The bending moment (M) depends on bending stiffness (EI), and the tension force (T) is dependent on the axial stiffness of cable material (EA) and the axial strain of elements (ϵ). The tension force and bending moment are defined as follows:

$$M = EI \frac{\partial \vec{R}}{\partial S_e} \times \frac{\partial^2 \vec{R}}{\partial S_e^2} \quad (2)$$

$$T = EA \epsilon$$

To determine the cable's dynamic response, the elements of the cable are converted into the number of concentrated masses, and the equations in each node were numerically solved using the boundary

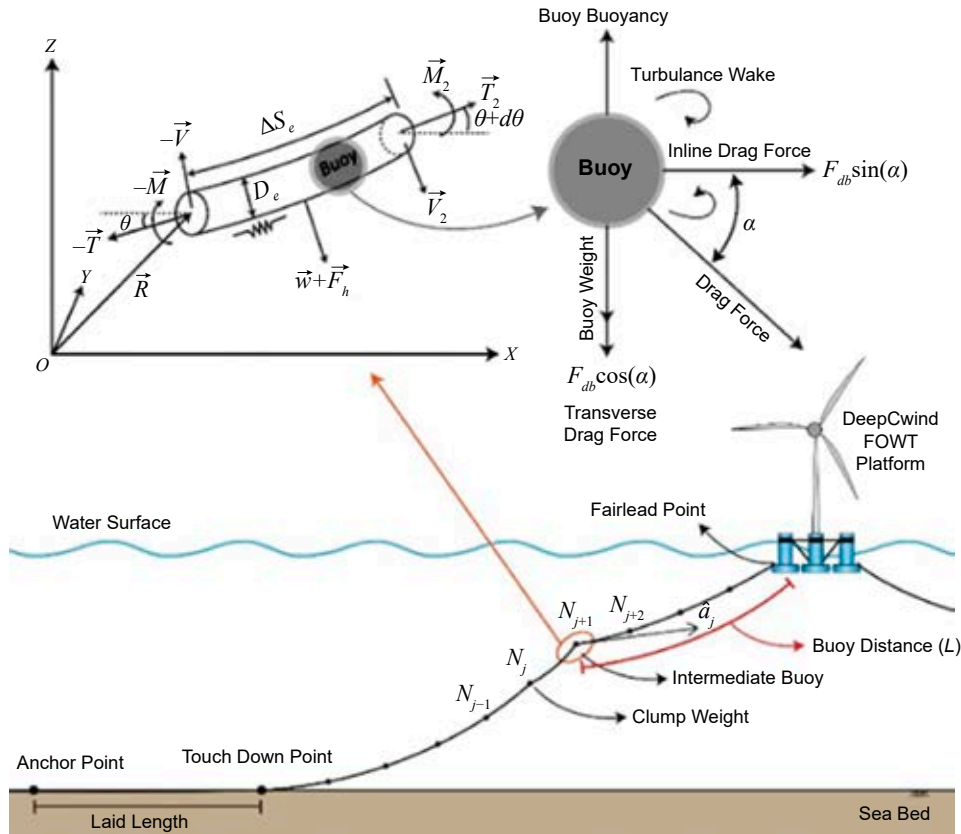


Figure 2. Modeling of a dynamic cable with an intermediate buoy

element method (BEM). We chose two pinned points at the top (\bar{P}_{top}) and bottom \bar{P}_{bottom} of the unstretched cable (L) as the boundary conditions, which are given as follows:

$$\begin{aligned} \bar{R}(0) &= \bar{P}_{bottom}, & \bar{R}(L) &= \bar{P}_{top} \\ \frac{\partial^2 \bar{R}(0)}{\partial S_e^2} &= 0, & \frac{\partial^2 \bar{R}(L)}{\partial S_e^2} &= 0 \end{aligned} \quad (3)$$

The unit axial vector of the j -th element, which is related to the slope of two adjacent elements, is equal to:

$$\hat{a}_j = \frac{\bar{R}_{j+1} - \bar{R}_j}{L_j}.$$

So, the unstretched element length with a good approximation is:

$$S_{e_j} \approx L_j = |\bar{R}_{j+1} - \bar{R}_j|.$$

Therefore, the curvature vector at point j (\bar{C}_j) is defined by the rate of slope change, which is calculated from the cross-product of unit vectors of the two adjacent elements. \bar{L}_j is the effective length of the j -th node which is defined as:

$$\bar{L}_j = \frac{L_j + L_{j-1}}{2}.$$

$$\bar{C}_j = -\frac{\partial \bar{R}}{\partial S_e} \times \frac{\partial^2 \bar{R}}{\partial S_e^2} \bigg|_j = \frac{1}{L_j} \hat{a}_j \times \hat{a}_{j-1} \quad (4)$$

With assuming the bending stiffness (EI) is constant between two adjacent elements, then Eqs. (2) and (4) lead to the bending moment at point j by:

$$\bar{M}_j = -(EI)_j \bar{C}_j \quad (5)$$

The axial (A_j) and normal (N_j) directional tensors are defined as follows:

For the general configuration of cables, the axial stiffness (EA) is much greater than the bending stiffness (EI), so assuming the distributed bending moment is zero, from Eqs. (1) and (6), the shear force matrix on the element j is expressed as:

$$\begin{aligned} A_j &= \hat{a}_j^T \hat{a}_j \\ N_j &= I - A_j \end{aligned} \quad (6)$$

$$[V_{(j)}] = -\frac{1}{L_j} N_j \left[(EI)_{j+1} \frac{1}{L_{j+1}} \hat{a}_{j+1} + (EI)_j \frac{1}{L_j} \hat{a}_{j-1}^T \right] \quad (7)$$

The element bending stiffness matrix was directly derived from the shear force as Eq. (8):

$$[dV] = [\nabla^T \vec{V}]^T [u] = -K_b [u] \quad (8)$$

From Eq. (7), it can be seen that the shear force on element j is a function of the four-node positions of $j-1, j, j+1$, and $j+2$ (for the elevation of \hat{a}_{j-1} and \hat{a}_{j+1} , which defined by $\hat{a}_j = (\vec{R}_{j+1} - \vec{R}_j) / L_j$). Accordingly, K_b is a 12×12 matrix. By indicating $[u_{j-1}]$, $[u_j]$, $[u_{j+1}]$, and $[u_{j+2}]$ as the motions at these four points, by substituting Eq. (7) into Eq. (8), the following equation can be expressed as follows:

$$[dV_{(j)}] = \sum_{m=j-1}^{j+2} [\nabla^T \vec{V}]^T [u_m] = \sum_{m=j-1}^{j+2} -K_m [u_m] \quad (9)$$

where:

$$K_m^T = \frac{1}{L_j} [\Xi_j \nabla_m]^T A_j + \left(\nabla_m^T \frac{1}{L_j} \right) \Xi_j^T N_j + \frac{1}{L_j} (\nabla_m^T \Xi_j^T) N_j \quad (10)$$

Concerning the displacement at node m ,

$$\nabla_m = \left(\frac{\partial}{\partial x}, \frac{\partial}{\partial y}, \frac{\partial}{\partial z} \right) \Big|_m$$

is the gradient operator, and is defined as

$$\Xi_j = - \left\{ (EI)_{j+1} \frac{1}{L_{j+1}} [\hat{a}_{j+1} - \hat{a}_j]^T - (EI)_j \frac{1}{L_j} [\hat{a}_j - \hat{a}_{j-1}]^T \right\} \quad (11)$$

The axial elastic force applied to element (j) is defined as a function of two-node deformation in the following form

$$-K_a \begin{bmatrix} [u_j] \\ [u_{j+1}] \end{bmatrix} = dF \quad (12)$$

where K_a is the 2×2 stiffness matrix of the mooring line element characterized as

$$K_a = \begin{bmatrix} K_{33} & -K_{33} \\ -K_{33} & K_{33} \end{bmatrix}, \text{ where } K_{33} = K_x A_j + \frac{T_j}{L_j} N_j \quad (13)$$

K_x is the inline linear stiffness or equivalent inline stiffness for a nonlinear axial stiffness cable. By bringing all elements matrices together and applying boundary conditions on the two attachment points of the mooring line, the static solution can be solved as Eq. (14).

$$K[u] = F_{\text{total}} \quad (14)$$

In time-domain analysis, the cable motion at given attachment locations can be obtained as

$$M[\ddot{u}] = F_{\text{total}} \quad (15)$$

where (F_{total}) and m are the assembled total force matrix and the total mass matrix (including structural and added masses), respectively.

Dynamic of multi-segment catenary mooring line with the intermediate buoy

By integrating both sides of Eq. (1) and applying the boundary conditions at the cable's ends, the j -th element motion response can be written in matrix form:

$$\begin{bmatrix} -T_j \hat{a}_j^T \\ -T_{j+1} \hat{a}_j^T \end{bmatrix} + \begin{bmatrix} -[V_j] \\ [V_{j+1}] \end{bmatrix} + \frac{L_j}{2} \begin{bmatrix} [\vec{w} + \vec{F}_h]^T \\ [\vec{w} + \vec{F}_h]^T \end{bmatrix} = \frac{mL_j}{2} \frac{\partial^2}{\partial t^2} \begin{bmatrix} \vec{R}_j^T \\ \vec{R}_{j+1}^T \end{bmatrix} \quad (16)$$

It is noted that the j in parentheses represents the element, and the j without parenthesis represents the node. $[V_j] = [V_{(j-1)}] - [V_{(j)}]$ is the shear force at node j , which is obtained by discretizing two adjacent elements. F_h is the hydrodynamic forces applied on the cable, which consist of a buoyancy force (F_b) and Morison force for the inline forces caused by the vibration of the body under stimulation of a wave and current. Morrison's force is divided into two parts: drag (F_d) and radiation force (F_r). The radiation force depends on the cable element added mass matrix (m_a) and acceleration of the cable (\vec{a}_j) at node j . The general form of hydrodynamic forces is given by the following equation:

$$F_h = F_b + F_d - m_a [\vec{a}_j, \vec{a}_{j+1}]^T \quad (17)$$

If the mass of an intermediate clump weight attached at node j is defined as M , and if there is no clump weight at the $j+1$ node, the total gravitational force in the element with the starting and ending nodes of j and $j+1$, is a 6×1 matrix in the fixed references axes. We assume that half of the gravitational force caused by the clump weight affects the adjacent element. g is gravitational acceleration, and the clump weight at nodes j and $j+1$ are given as follows:

$$w = (\vec{w}_j, \vec{w}_{j+1})^T = \left\{ 0, 0, -\frac{1}{2} (mL_j + M)g, 0, 0, -\frac{1}{2} mL_j g \right\}^T \quad (18)$$

It was assumed that there is a clump weight at node j and an intermediate buoy at node $j+1$. Indicating the displaced mass of water of intermediate buoy as M_b , and the equivalent cross-sectional area of mooring line as A_{cj} , the element buoyancy force matrix is defined as:

$$F_b = \left\{ 0, 0, \frac{1}{2} \rho_w A_{cj} L_j g, 0, 0, 0, \frac{1}{2} (\rho_w A_{cj} L_j + M_b) g \right\}^T \quad (19)$$

where ρ_w is the density of water. The simplified form of the drag force applied to the mooring line element in the time domain is given by:

$$F_d(t) = \left\{ \begin{array}{l} f_d(j) - \frac{1}{2} C_{dc} S_c \rho_w |U_j(t) - V_j(t)| \{U_j(t) - V_j(t)\} \\ f_d(j+1) + \\ - \frac{1}{2} C_{db} S_b \rho_w |U_{j+1}(t) - V_{j+1}(t)| \{U_{j+1}(t) - V_{j+1}(t)\} \end{array} \right\} \quad (20)$$

where $V_j(t) = \{V_{x_j}(t), V_{y_j}(t), V_{z_j}(t)\}^T$ is the shape matrix of the mooring line velocity at node j at time t , and $U_j = \vec{U}_j^T = \{U_{x_j}, U_{y_j}, 0\}^T$ is the matrix form of the current velocity at the location of node j . C_{dc} and C_{db} are the drag coefficients of the clump weight (attached at node j) with projected surface areas of S_c and the intermediate buoy (attached at node $j+1$) with projected surface areas of S_b , respectively. The drag force on the mooring line element ($f_d(j)$) is expressed as

$$f_d(j) = -\frac{1}{4} C_x \rho_w D_j L_j |A_j \{U_j(t) - V_j(t)\}| A_j \{U_j(t) - V_j(t)\} + -\frac{1}{4} C_d \rho_w D_j L_j |N_j \{U_j(t) - V_j(t)\}| N_j \{U_j(t) - V_j(t)\} \quad (21)$$

where C_d and C_x are the transverse and inline drag coefficients, respectively.

To obtain proper results, the drag force along the cable element should be integrated to consider variations in the current velocity along with the element. In this paper, the Gaussian numerical integration method was used to calculate this integral.

Methodology of research

In this research, the process was based on the OC4-DeepCwind semi-submersible FOWT platform

(Robertson et al., 2014). Numerous experiments have been carried out by using the 5 MW baseline wind turbine developed by NREL (Coulling et al., 2013; Goupee et al., 2014; Liu et al., 2019). An overview of the NREL-FAST structure including the various modules and datasets of the input and output analysis process was provided by Imani et al. (Imani et al., 2020). The platform was designed for a 200-meter water depth. The mooring lines consist of three catenary steel chain cables 120° to each other, as depicted in Figure 3. Table 1 shows the specifications of the mooring lines.

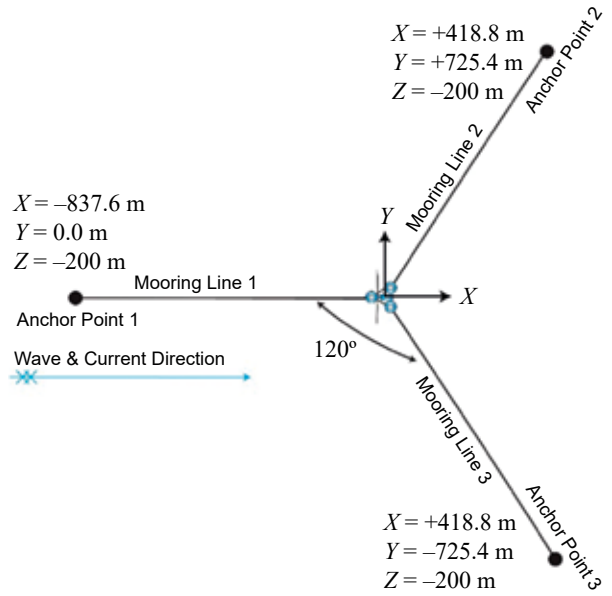


Figure 3. Plan of mooring system and anchor points coordinates

Table 1. Mooring line properties

Unstretched Mooring Line Length (m)	835.5
Radius to Anchors from Platform Centerline (m)	837.6
Chain Diameter (m)	0.0766
Equivalent Mass per Unit Length (kg/m)	108.63
Axial Stiffness (EA) (N)	753,600,000
Tensile Strength (N)	5,454,000
Longitudinal Drag Coefficient	0.025

To improve the performance of the DeepCwind mooring line system, catenary cables were divided into two different segmentations, and an intermediate buoy was attached at the catenary segment joints. The material properties of the cables were considered to be the same on both sides of the joint. Six spherical buoy devices with different radiuses of 0.8, 1.0, 1.2, 1.4, 1.6, 1.8, and 2.0 meters with different added masses, displaced water, and drag coefficients were selected. The reason for choosing

a high volume of buoys was to provide horizontal stiffness to prevent a large offset of the platform (Gao & Moan, 2009). Each of these buoys was individually connected along three cables at six distances of 100, 200, 300, 400, 500, and 600 meters from the fairlead point. The cables were converted into two different segments, and the buoy was at its intersection joint. Figure 4 shows the configuration of mooring lines by arranging different buoys simultaneously at different distances. The difference between the sizes of buoys on the mooring system configuration is well illustrated. The buoys at the joints positively raised the cable. The rise was further increased upon increasing the buoy radius due to increased buoyancy and because it bore part of the cable weight. Also, as the buoy approached the anchor point, the angle of joint segments increased. In this figure, R represents the radius of buoys, and L indicates the horizontal distance between the centers of the buoy to the fairlead point on the platform. The full-scale platform with mooring line systems was modeled in ANSYS-AQWA software, and the simulations were performed in harsh offshore conditions with the 50-year return period load cases based on ultimate limit state (ULS) design criteria shown in Table 2. This simulation was based on the boundary element method (BEM) and was conducted by

Table 2. Environmental conditions

Wave Properties	
Wave Type	Stokes 2 nd -Order Wave Theory
Propagation Direction	0° (Parallel to Turbine Hub)
Wave Height (m)	8
Period (s)	9.43
Frequency (Hz)	0.106
Current Properties	
Distribution method	Exponentially in Depth
Propagation Direction	0° (Parallel to Turbine Hub)
Variation Inverse Exponent	2
Velocity at the free surface of water (m/s)	1.06
Velocity at Depth of 100 meter (m/s)	0.75

utilizing three-dimensional radiation/diffraction theory (Motallebi et al., 2020) and Morison’s equation (hybrid method) in regular waves in the frequency and time domain.

Validation

To calibrate the numerical model and validate the results of the ANSYS-AQWA simulation, the results

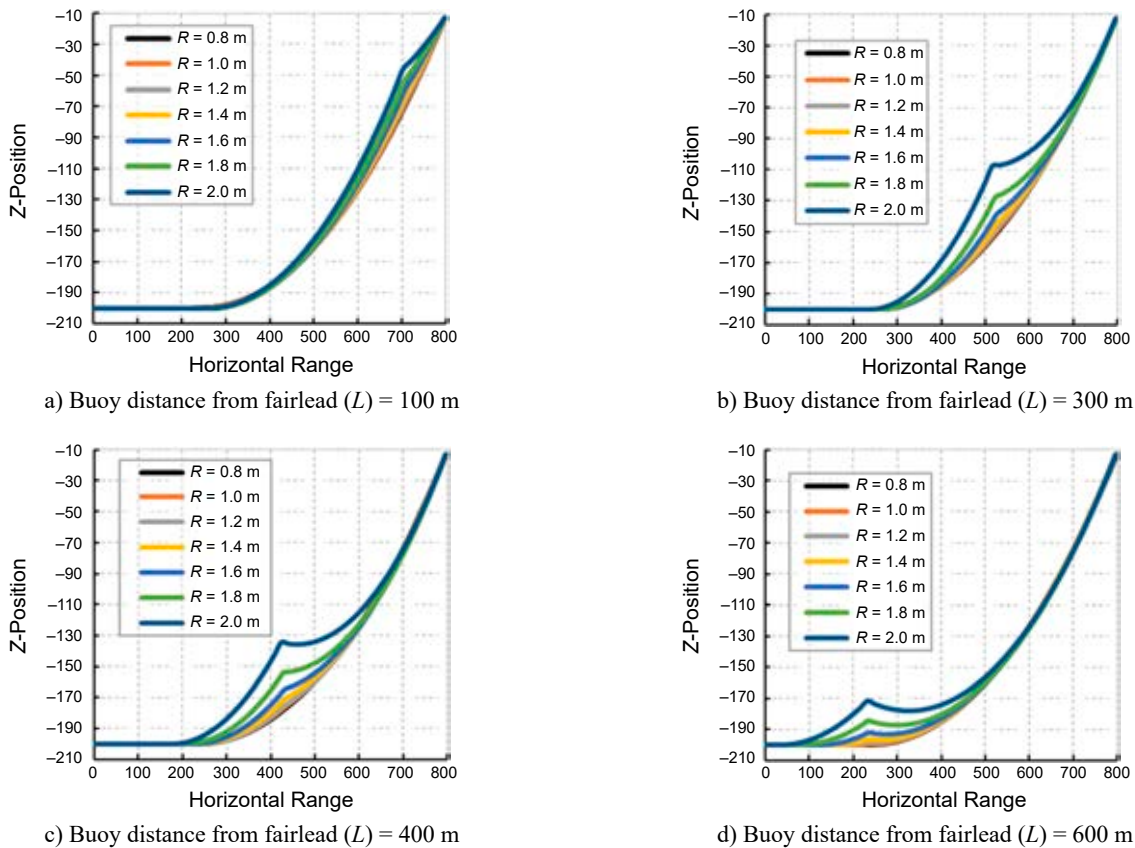


Figure 4. Configurations of mooring lines by the effect of different buoys

of the 1:50 scale model of the OC4-DeepCwind platform laboratory test were used. The platform was tested under wind and wave load cases in the Maritime Research Institute Netherlands (MARIN) in 2011 (Masciola et al., 2013). Based on these results, Hall and Goupee (Hall & Goupee, 2015) validated the lumped mass mooring line model. By using an NDI Certus optical motion tracking system, they recorded the platform's motions. The results of this validation were based on the regular waves in accordance with $H_s = 10.3$ m and $T_s = 12.1$ s, which were similar to the laboratory conditions. Figure 5 shows the ANSYS-AQWA simulation model and the laboratory model of the DeepCwind platform. Shokouhian et al. (Shokouhian et al., 2019) employed the ANSYS-AQWA software package and extracted the hydrodynamic responses of semi-submersible

FOWT DeepCwind platform and validated the model with the MARIN experimental results. They explained that the average heave, surge, and cable tension forces of the AQWA model were 15.5% closer to the test results than those from the FAST program.

The numerical model validation was carried out in two stages: 1) Based on platform motions and 2) Fairlead cable tension. Figure 6 illustrates the comparison between the experimental data and the ANSYS-AQWA numerical results of the platform motions for surge, heave, and pitch. Acceptable agreement in amplitudes between the numerical model and the test data is evident, although, in heave and pitch motions, the model predicted a higher excitation between peaks. The results of the time history of fairlead point tension for test and numerical model



a) Scaled model of OC4-DeepCwind platform in MARIN (Hall & Goupee, 2015)



b) Simulated model of OC4-DeepCwind platform

Figure 5. Simulation and laboratory model of OC4-DeepCwind platform

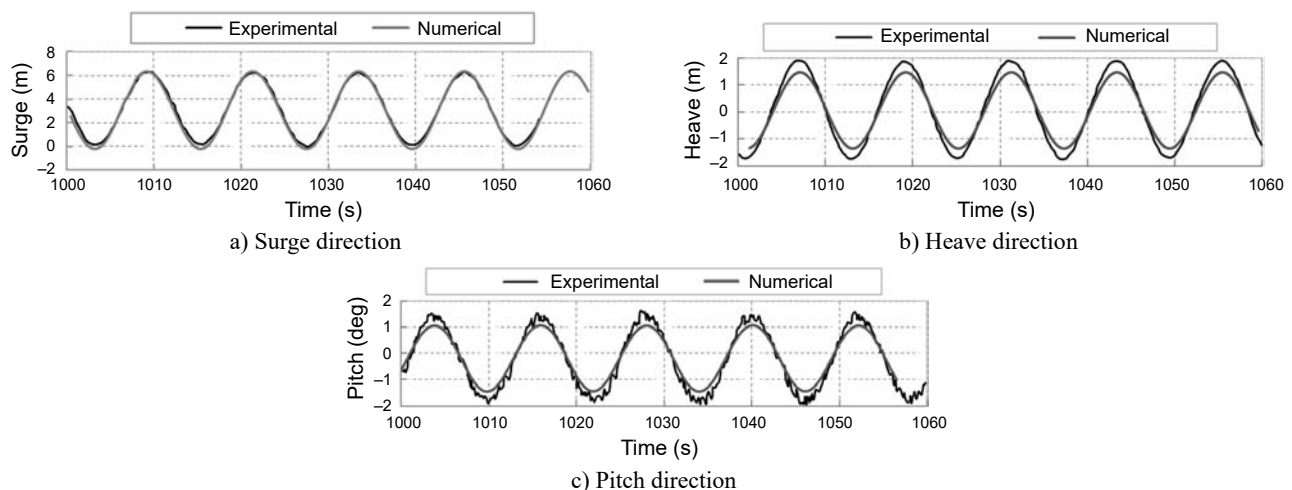


Figure 6. Experimental and numerical comparison of platform motions

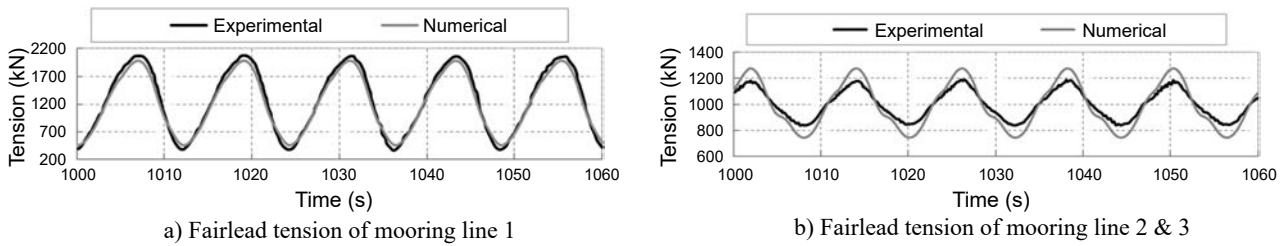


Figure 7. Experimental and numerical comparison of fairlead tension

are presented in Figure 7. The comparison shows an accuracy close to 95% between the numerical model and experimental results. These discrepancies were assigned to the different techniques adopted in hydrodynamic simulations, such as a discrepancy in the viscous-drag coefficients, Froude similarity procedure, ignoring the effects of second-order wave forces, or even different mooring line models.

Results and discussion

In this study, a hybrid method in ANSYS-AQWA software based on the combination of panels and Morison elements was employed to model the semi-submersible DeepCwind FOWT platform with a nonlinear multi-segment catenary mooring line and intermediate buoy. The surface of the full-scale floating body was divided into 12,474 quadrilateral

and triangular panels. The results will be examined in three sections of mooring line’s strain, tension, and uplift. The mooring lines used in this study exhibited nonlinear behavior due to tension-dependent Young’s modulus of the mooring chains (Tahar & Kim, 2008).

According to the arrangement of the mooring lines (Figure 3), mooring line 1 will probably be exposed to a greater force than other mooring lines due to the 0° incidence (parallel to turbine hub) between the wave and current. Also, since the platform is symmetric about the longitudinal axis, mooring lines 2 and 3 are also symmetrical. Therefore, only the answers for mooring line 2 are provided. In the next section, we present and discuss the results of the strain, anchor uplift, and platform motions on different buoys sizes and different positions along the cable.

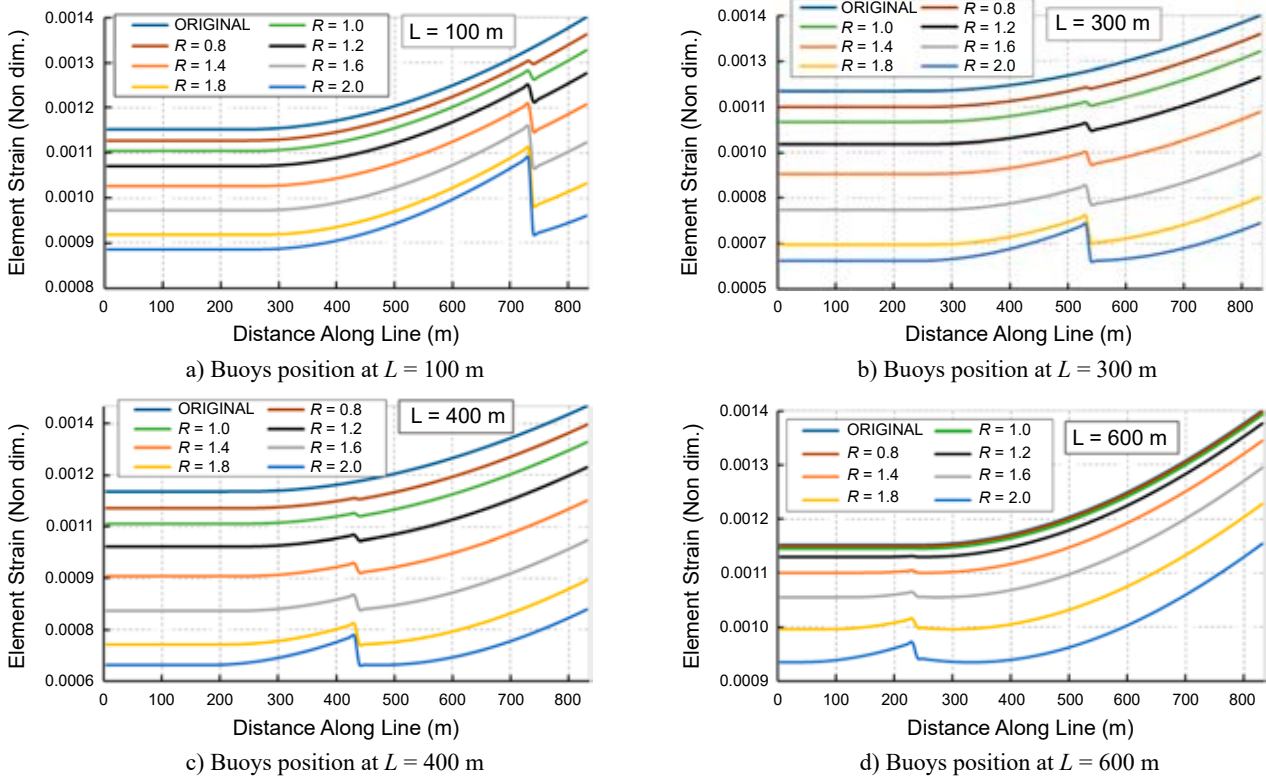


Figure 8. Variations of cable strain against different buoy positions and radiuses

Elements strain along mooring lines

Due to its elasticity, the cable length may be stretched due to the tensile forces caused by the movement of the platform. In fact, the strain of the cable is a non-dimensional ratio of cable elongated length to the actual length of the cable ($\varepsilon = (S_e - S_{e0})/S_{e0}$). Steel chains are subjected to cyclic loads, loading, and offloading. Therefore, due to the low elasticity of the steel chains, permanent plastic strain occurred, and cracks began to grow at notches and eventually resulted in fracture. Figure 8 illustrates the strain variations of mooring line 1 under the environmental conditions of the problem. As can be seen in this figure, at all buoy placements, the strain along the cable decreased by varying the buoy size. The larger the buoy size, the lower the strain along the cable, and the higher the strain drop rate. In this figure, L indicates the horizontal distance between the centers of the buoy to the fairlead point on the platform. The “Original” model refers to the mooring lines of the DeepCwind platform without a buoy. Table 3 compares the strain reduction percentage at the anchor and fairlead points of the cables. The results show that when the buoy approaches the center of the cable, the buoy has a more evident strain-reducing effect. Placing the buoy 300 m from the fairlead point had the best influence, so that over 90% helped reduce the mooring line strain.

Tension

One of the most important parameters of the mooring line design and fatigue analysis is cable tension. Tension is defined as the tensile force applied to the mooring lines and also the nonlinear dynamic coupling between the six degrees of freedom of the platform and mooring lines. Material properties, stress-strain relationship, and restoring stiffness of lines also affect a cable’s predicted dynamic response (Tang et al., 2007). Increasing applied cyclic tension and ramping inline tensions in mooring lines leads to the formation of cracks in the chains of catenary mooring lines. The tensile cracks are mostly perpendicular to the loading direction, so that when they reach a critical length, the mooring line abruptly fails without warning (Cook & Young, 1999). Connecting a buoy increases the geometric compliance and flexibility of the mooring line and is a simple way to reduce the risk of cable failure. Figure 9 shows the tension variations of cable elements versus different buoy positions and radiuses. Figure 10 indicates the time history of the cable tension

Table 3. Strain reduction under each condition

L	Percentage of strain reduction at the anchor point							
	R							
	0.8	1	1.2	1.4	1.6	1.8	2	
100	-2.20	-4.33	-7.59	-12.27	-18.44	-25.40	-30.00	
200	-3.89	-7.87	-14.33	-24.45	-39.70	-59.43	-71.67	
300	-4.76	-9.69	-17.84	-30.95	-51.28	-77.78	-93.88	
400	-4.39	-8.87	-16.06	-27.08	-42.99	-62.74	-77.86	
500	-2.76	-5.55	-9.95	-16.55	-25.85	-37.70	-49.16	
600	-0.16	-0.58	-1.98	-4.69	-9.19	-15.67	-23.24	
L	Percentage of strain reduction at the fairlead point							
	100	-2.80	-5.51	-9.74	-15.98	-24.70	-35.67	-45.80
	200	-3.99	-8.09	-14.79	-25.38	-41.74	-64.40	-83.49
	300	-4.58	-9.25	-16.94	-29.25	-48.36	-74.21	-94.90
	400	-4.02	-8.09	-14.58	-24.42	-38.58	-56.56	-72.95
	500	-2.47	-4.95	-8.86	-14.69	-22.90	-33.55	-44.93
	600	-0.14	-0.51	-1.76	-4.16	-8.19	-14.07	-21.37

for mooring lines 1, 2, and 3. All figures show the positive role of buoys in diminishing the cable tension. As the buoy size increases, the damping trend of cable fluctuations also intensifies and stabilizes. According to Figure 10, from 100 m to 400 m of the buoy position, upon increasing the buoy size, mooring line oscillations from the harmonic steady-state gradually transformed to the transient and damped vibration form. This technique eliminates cyclic oscillations and strongly reduces the risk of fatigue failure. When the buoy dimensions increased, the thickness of the wake turbulence layer behind the buoy also increased. This increased the drag coefficient of the buoy and, consequently, increased the drag force of the cable at the buoy’s position, which led to abundant cable resistance against the applied forces. Figure 11 shows the polynomial regression of mooring line tension versus different buoy volumes. The positive effect of the buoy at reducing tension is evident in all cases. The highest depreciation rates for mooring lines 2 and 3 occurred at a distance of 300 m and at a radius of 2 m at which, the cable tension was reduced by up to 45%. Also, the effectiveness of the buoys at reducing the tension of mooring line 1 was less than that of mooring lines 2 and 3, which at best reduced the cable tension by 30% at a buoy distance of 400 m.

Anchor uplift

The anchor uplift force is the vertical (upward) component of the tension at the connection point to the sea bed. This force is equal to the cable’s buoyancy force. When the buoy is attached to the

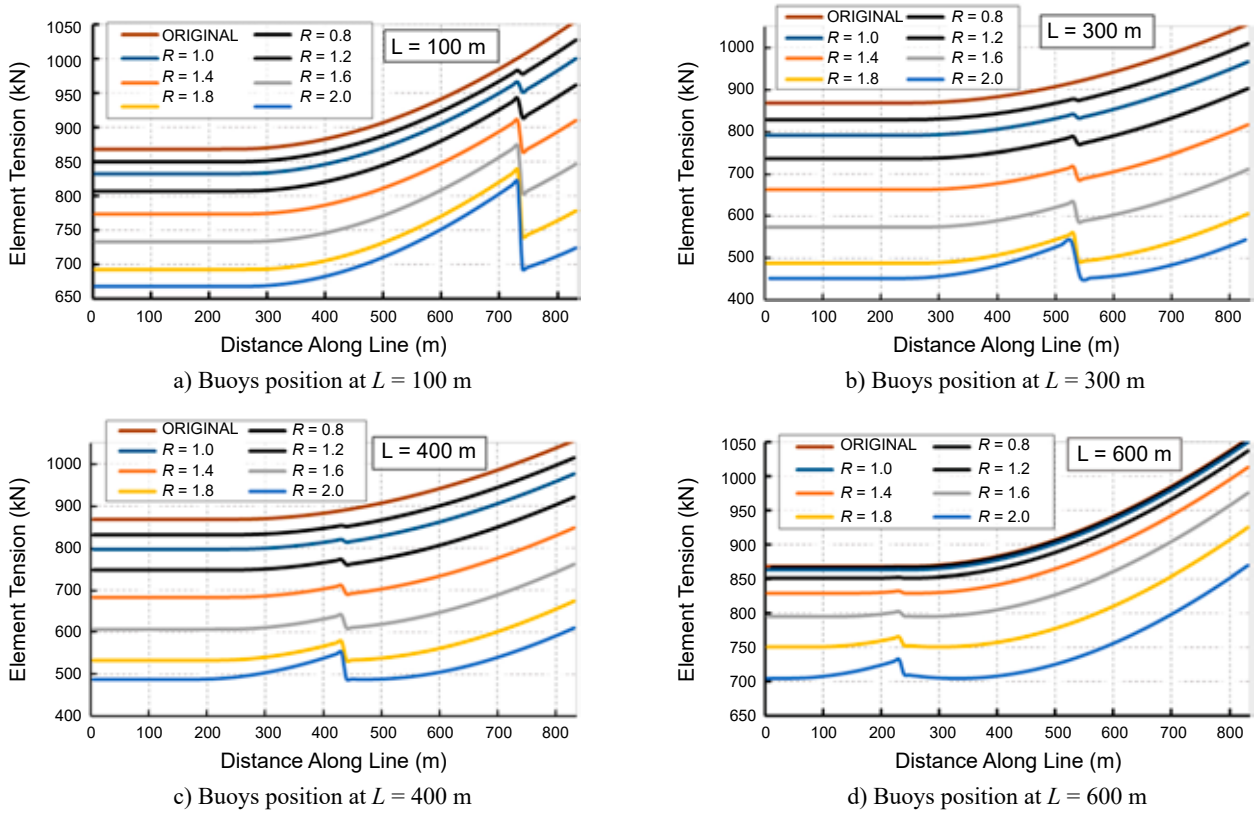


Figure 9. Variations of tension of cable elements against different buoy positions and radiuses

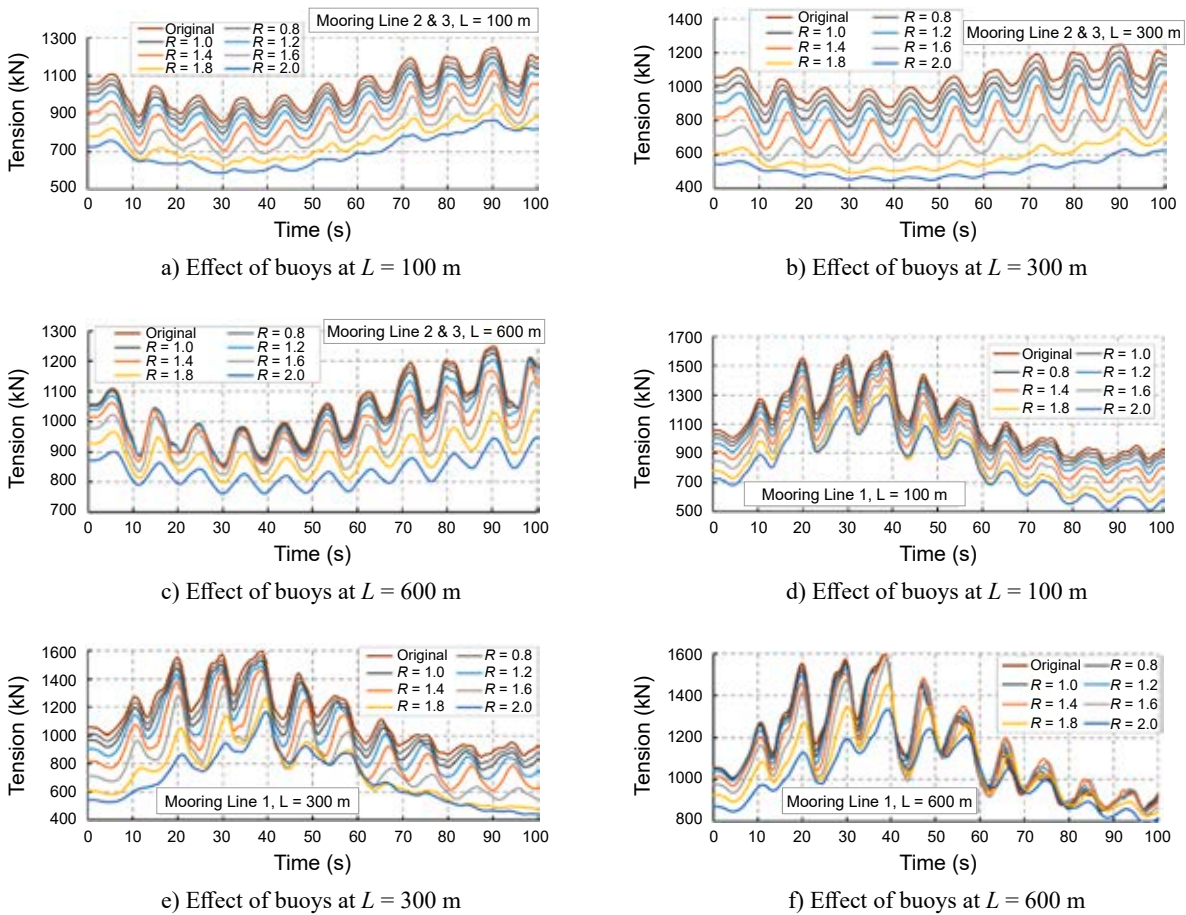


Figure 10. Time history of mooring lines 1, 2, and 3 tension versus different buoy positions and radiuses

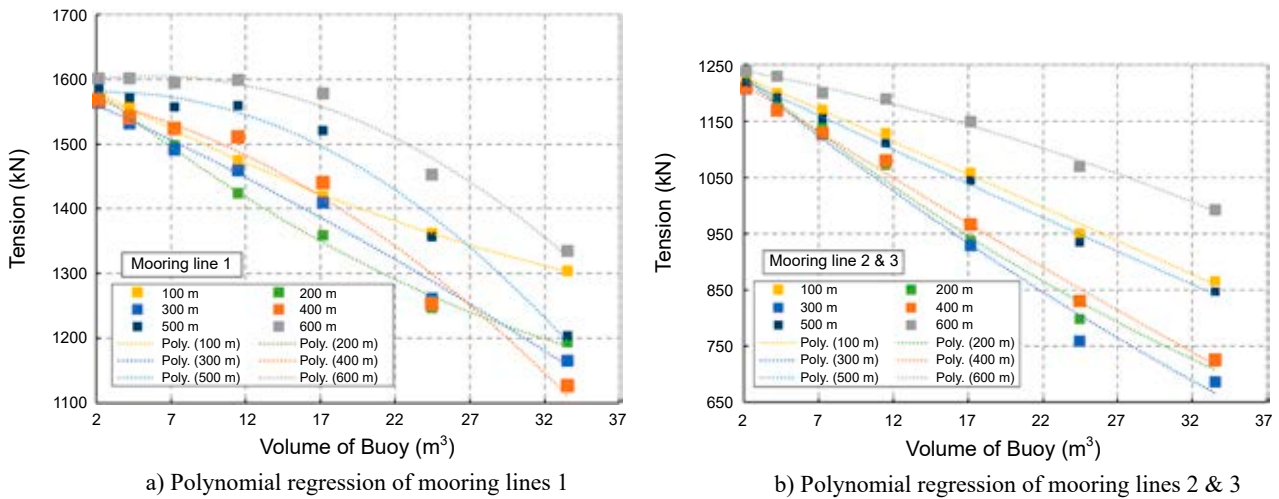


Figure 11. Polynomial regression of mooring line tension versus buoy volume

mooring system, depending on the installation position, it will add positive or negative buoyancy to the attachment points. Figure 12 shows the time history of the anchor uplift at different positions. Figure 13 summarizes the obtained results compared with the original mooring line configuration. The results show from the fairlead point up to 300 m buoy position along the cable. Due to the dominance of the cable and buoy's gravitational weight and inline drag terms, the anchor uplift decreased so that by placing the buoy with a 1.8 m radius at a distance

of 200 m, the uplift force was reduced by up to 70% and 95% for mooring lines 1 and 2 (or 3), respectively. However, as the buoy passed a distance of 300 m, the transverse component of the tension and drag force, due to buoy and cable density, increased the vertical forces. On the other hand, the buoy will tolerate a part of the cable's weight and reduce the gravity force of the cable. As a result, by placing the buoy with a radius of 2 m at a distance of 600 m, we observed a 30-times increase in the anchor uplift force.

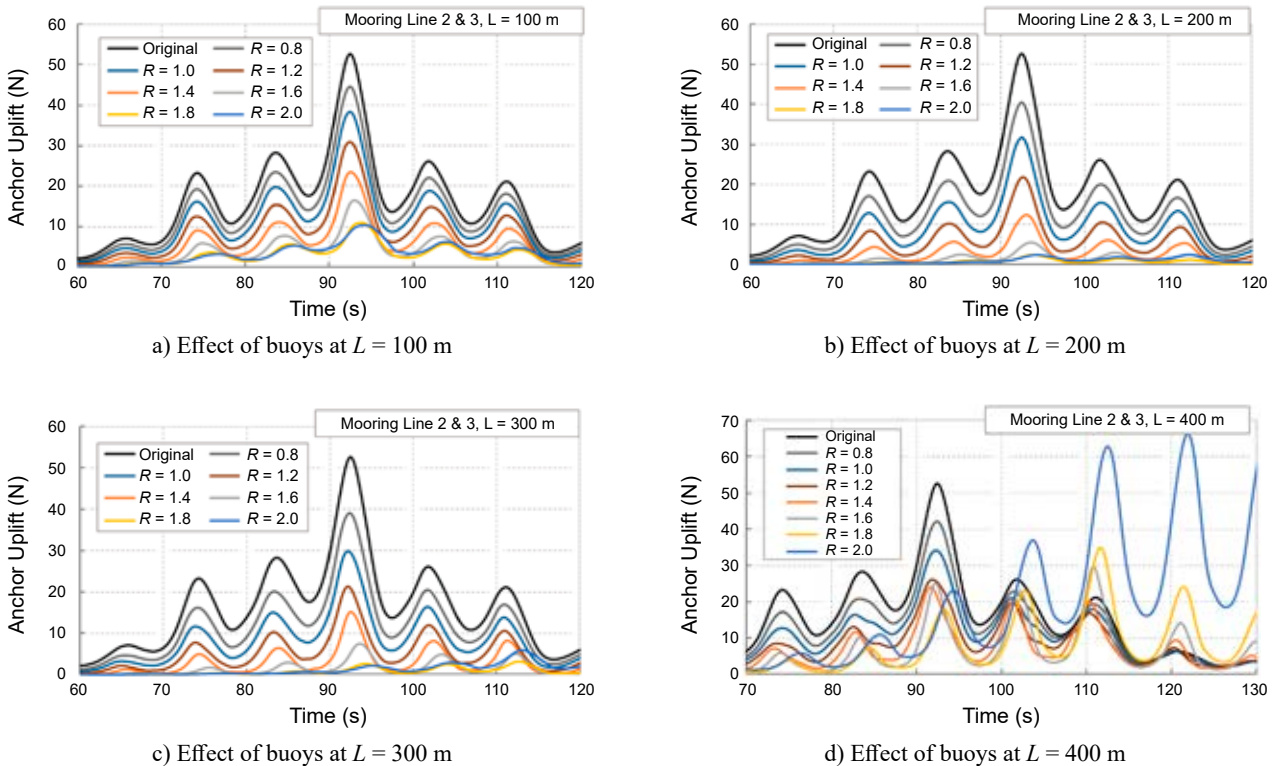


Figure 12. Time history of mooring lines 2 and 3 uplift versus different buoy positions and radiuses

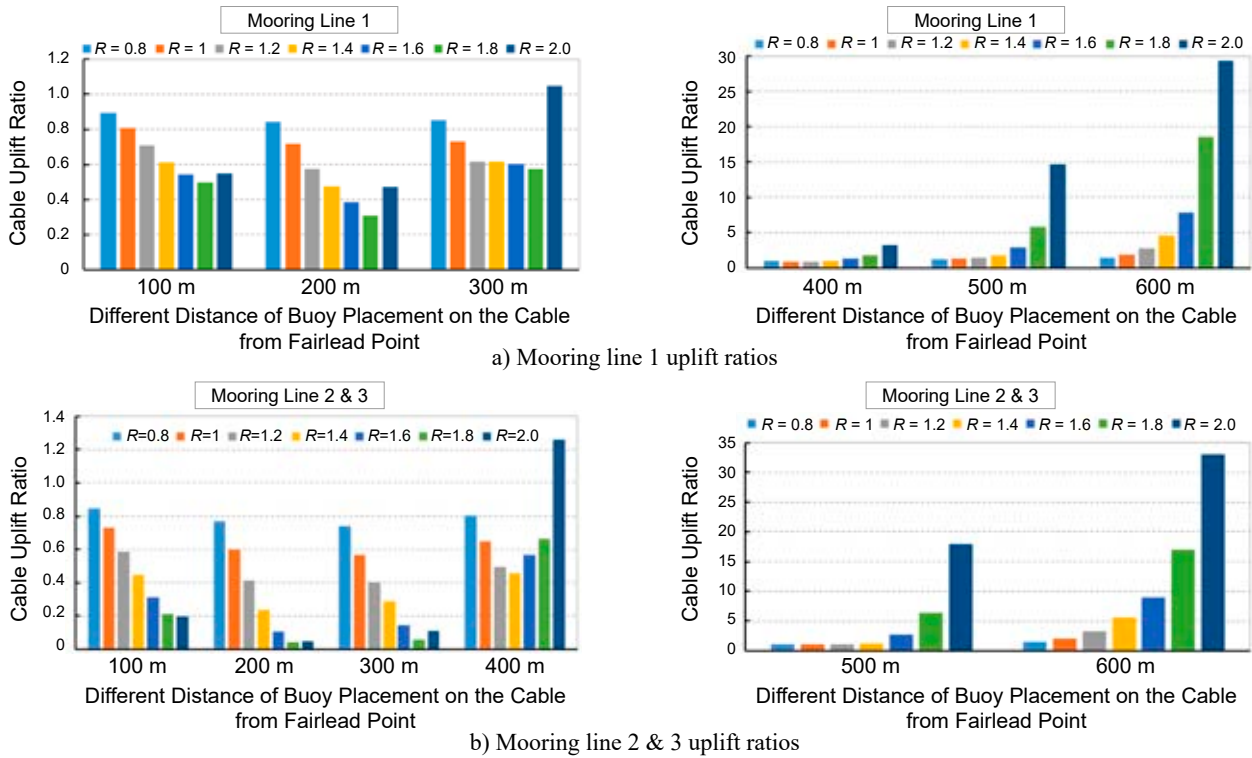


Figure 13. Ratios of anchor uplift with buoy compared with the non-buoy mode

Platform motion

Fully-coupled time-responses of OC4-Deep-Cwind platform (surge, heave, and pitch motions at CG) where the buoy with 2 m radius was placed at different positions of the mooring system are shown

in Figure 14. A summary of the platform motion changes under different conditions was compared to the original model and is presented in Table 4. The variations in Table 4 are strongly dependent on the buoy size. By increasing the radius of the buoy from 0.8 m to 1.2 m at different positions in three directions

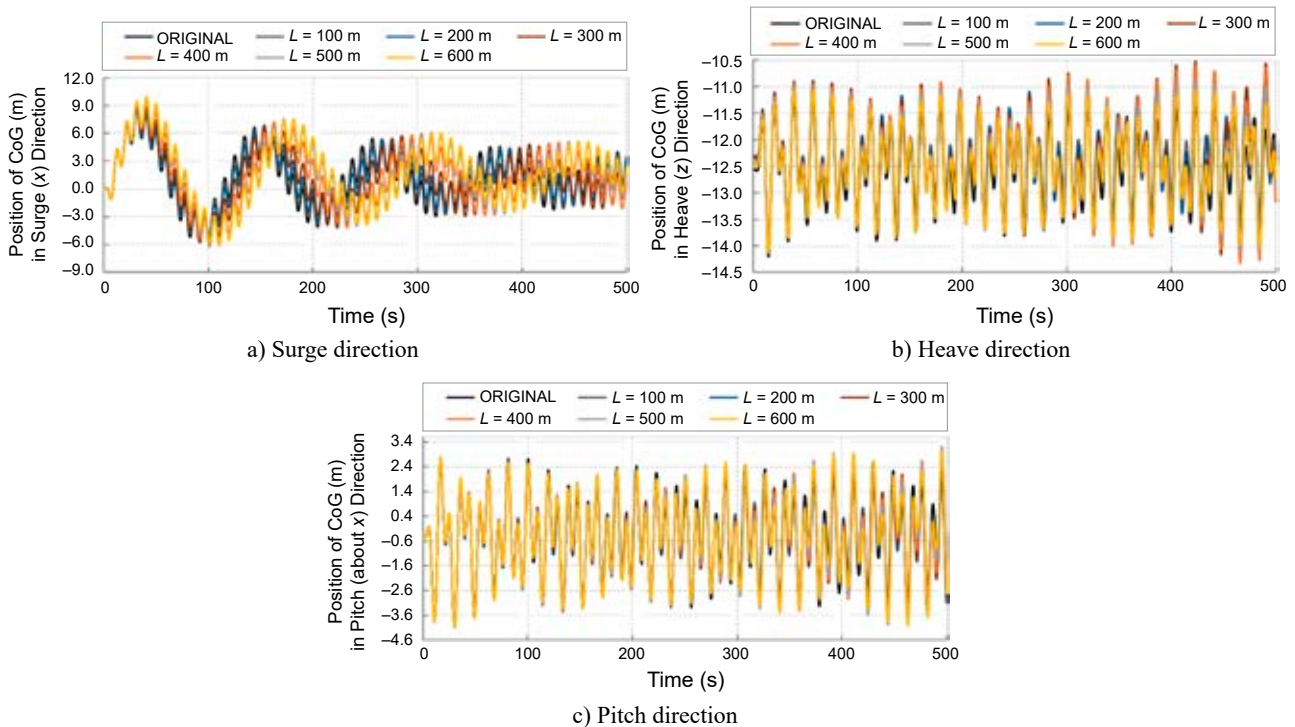


Figure 14. Time history of motion responses in different distances of buoy placement on the cable from fairlead point

Table 4. Motion variations under each condition

L	Percentage of motion amplitude changes compared to the original model						
	R						
	0.8	1	1.2	1.4	1.6	1.8	2.0
	Surge (x)						
100	-0.28	-0.51	-0.83	-1.12	-0.62	+1.66	+5.22
200	-0.50	-0.95	-1.66	-2.07	+0.10	+5.81	+16.90
300	-0.73	-1.34	-1.98	-1.54	+5.12	+17.75	+34.19
400	-0.29	-0.47	-0.66	+1.76	+9.81	+25.22	+42.32
500	+0.64	+0.82	+2.55	+5.33	+11.62	+22.76	+37.05
600	+0.74	+1.16	+3.37	+7.14	+12.24	+20.01	+29.65
	Heave (z)						
100	-0.09	-0.23	-0.29	-0.29	+0.06	+0.52	+0.99
200	-0.16	-0.29	-0.43	-0.29	+0.43	+1.55	+3.67
300	-0.16	-0.29	-0.39	-0.16	+0.82	+1.98	+20.04
400	-0.09	-0.16	-0.26	-0.23	0.49	+3.53	+23.65
500	+0.03	0	+0.16	+0.92	+3.30	+4.13	+8.03
600	+0.06	+0.09	+0.16	+2.08	+3.07	+4.03	+5.66
	Pitch (about y)						
100	-0.11	-0.08	+0.01	-0.04	-0.57	-0.79	+0.53
200	-0.23	-0.45	-0.84	-1.48	-1.90	-0.66	+11.08
300	-0.31	-0.61	-1.15	-1.87	-0.86	+2.83	+38.32
400	-0.17	-0.31	-0.54	-0.84	+3.81	+7.51	+34.09
500	+0.11	+0.18	+1.35	+3.55	+6.71	+7.93	+14.85
600	+0.11	+0.30	+0.66	+2.95	+3.71	+7.13	+14.19

of surge, heave, and pitch, there was no noticeable change in platform motion. Most of the major changes in platform motion occurred when the buoy was positioned between 300 and 400 meters, roughly in the middle of the mooring line. Within a radius of 2 m for the buoy, the range of motion increased to its maximum, so that within 400 meters of the buoy's position, the amplitude of motion increases to 42%, 23%, and 34% in surge, heave, and pitch degrees of freedom, respectively.

Conclusions

In this study, the mechanical behavior of DeepCwind semi-submersible FOWT platform mooring lines was investigated. The nonlinear catenary mooring lines of the platform were divided into two segments and an intermediate buoy device was attached at catenary segment joints. The tension, anchor uplift, strain at different buoy radiuses, and its position along cable were presented in detail. Moreover, the platform motion in three directions (heave, pitch, and yaw) was analyzed. The results of the study led to the following conclusions:

- When the buoy device was mounted on the cable, the cable was raised positively due to the greater

cable buoyancy and because it bore part of the cable's weight. A larger buoy size increased the cable lift. Also, as the buoy approached the anchor point, the angle of the joint segments increased.

- Placing the buoy 200 m to 400 m away exerted the greatest strain reduction at both fairlead and anchor points, which enabled the mooring lines to reduce the strain by 90%.
- As the buoy radius increased to 2 m, the strain decreased along the cable, and the strain drop rate was greater.
- By increasing the buoy radius to 2 m, the tension stimulations from the harmonic steady-state became a damped vibration form and eliminated cyclic oscillations and strongly reduced the risk of fatigue.
- The existence of a buoy at a distance between 200–300 m had a greater effect on reducing the mooring line's tension rate. When the distance was 300 m, and the radius of the buoy was 2 m, the cable tension was reduced by 45%.
- Positioning the buoy at a horizontal distance of 400 m to 600 m from the fairlead led to a sharp increase in the uplift force.
- By increasing the radius of the buoy to 1.2 meters at different points, there was no noticeable variation in the platform's motion.
- Most of the major changes in the platform's motion were due to the positioning of the buoy in the middle of the mooring line.
- The wrong choice of buoy position can increase the platform's horizontal offset by up to 42%.
- Taking all aspects into account, positioning the buoy with a radius of 1.8 m at a distance of 200 m from the fairlead point was the best configuration in terms of improving the dynamic responses of the platform mooring line.

Overall, the numerical results demonstrated that the proposed multi-segment catenary mooring line with an intermediate buoy will improve the mooring line's mechanical performance. Nonetheless, the mentioned system will cause more complex dynamic properties and increase the installation difficulties in deep water.

References

1. AZCONA, J., MUNDUATE, X., GONZÁLEZ, L. & NYGAARD, T. (2016) Experimental validation of a dynamic mooring lines code with tension and motion measurements of a submerged chain. *Ocean Engineering* 129, pp. 415–427, doi: 10.1016/j.oceaneng.2016.10.051.
2. BAE, Y.H., KIM, M.H. & KIM, H.-C. (2017) Performance changes of a floating offshore wind turbine with broken mooring line. *Renewable Energy* 101, pp. 364–375.

3. BROWN, D.T. & MAVRAKOS, S. (1999) Comparative study on mooring line dynamic loading. *Marine Structures* 12 (3), pp. 131–151, doi: 10.1016/S0951-8339(99)00011-8.
4. COOK, R.D. & YOUNG, W.C. (1999) *Advanced Mechanics of materials*. Second Edition. New Jersey: Prentice Hall.
5. COULLING, A.J., GOUPEE, A., ROBERTSON, A., JONKMAN, J.M. & DAGHER, H.J. (2013) Validation of a FAST semi-submersible floating wind turbine numerical model with DeepCwind test data. *Journal of Renewable and Sustainable Energy* 5(2), p. 023116, doi: 10.1063/1.4796197.
6. DESSI, D., CARCATERRA, A. & DIODATI, G. (2004) *Experimental investigation versus numerical simulation of the dynamic response of a moored floating structure to waves*. *Journal of Engineering for the Maritime Environment* 218 (3), pp. 153–165, doi: 10.1243/1475090041737949.
7. GAO, Z. & MOAN, T. (2009) *Mooring system analysis of multiple wave energy converters in a farm configuration*. Proceedings of the 8th European Wave and Tidal Energy Conference, Uppsala, Sweden.
8. GHAFARI, H. & DARDEL, M. (2018) Parametric study of catenary mooring system on the dynamic response of the semi-submersible platform. *Ocean Engineering* 153, pp. 319–332, doi: 10.1016/j.oceaneng.2018.01.093.
9. GOUPEE, A.J., FOWLER, M.J., KIMBALL, R.W., HELDER, J. & DE RIDDER, E.-J. (2014) *Additional Wind/Wave basin testing of the DeepCwind semi-submersible with a performance-matched wind turbine*. Proceedings of the 33rd International Conference on Ocean, Offshore and Arctic Engineering, 8–13 June, 2014, San Francisco, California, USA.
10. HALL, M. & GOUPEE, A. (2015) Validation of a lumped-mass mooring line model with DeepCwind semisubmersible model test data. *Ocean Engineering* 104, pp. 590–603, doi: 10.1016/j.oceaneng.2015.05.035.
11. IMANI, H., ABBASPOUR, M., TABESHPOUR, M.R. & KARIMIRAD, M. (2020) *Effects of motion and structural vibration-induced loadings on the coupled dynamic response of a mono-column tension-leg-platform floating wind turbine*. *Journal of Engineering for the Maritime Environment* 234, 2, pp. 426–445, doi: 10.1177/1475090219882604.
12. KARIMI, M., BUCKHAM, B. & CRAWFORD, C. (2019) A fully coupled frequency domain model for floating offshore wind turbines. *Journal of Ocean Engineering and Marine Energy* 5 (2), pp. 135–158, doi: 10.1007/s40722-019-00134-x.
13. KWAN, C.T. & BRUEN, F.J. (1991) Mooring line dynamics: comparison of time domain, frequency domain, and quasi-static analyses. Paper presented at the Offshore Technology Conference, Houston, Texas, 6–9 May, 1991, doi: 10.4043/6657-MS.
14. LEE, K.-H., HAN, H.-S. & PARK, S. (2015) Failure analysis of naval vessel's mooring system and suggestion of reducing mooring line tension under ocean wave excitation. *Engineering Failure Analysis* 57, pp. 296–309.
15. LIU, Z., FAN, Y., WANG, W. & QIAN, G. (2019) Numerical Study of a Proposed Semi-Submersible Floating Platform with Different Numbers of Offset Columns Based on the DeepCwind Prototype for Improving the Wave-Resistance Ability. *Applied Sciences* 9(6), 1255.
16. MARTINEZ PEREZ, I., CONSTANTINESCU, A., BASTID, P., ZHANG, Y.-H. & VENUGOPAL, V. (2019) Computational fatigue assessment of mooring chains under tension loading. *Engineering Failure Analysis* 106, 104043, doi: 10.1016/j.engfailanal.2019.06.073.
17. MASCIOLA, M., ROBERTSON, A., JONKMAN, J., COULLING, A.J. & GOUPEE, A. (2013) *Assessment of the importance of mooring dynamics on the global response of the DeepCwind floating semisubmersible offshore wind turbine*. Proceedings of the 23rd International Offshore and Polar Engineering Conference, Anchorage, Alaska, USA, June 30–July 5, 2013, pp. 359–368.
18. MOTALLEBI, M., GHAFARI, H., GHASSEMI, H. & SHOKOUHIAN, M. (2020) Calculating the second-order hydrodynamic force on fixed and floating tandem cylinders. *Scientific Journals of the Maritime University of Szczecin, Zeszyty Naukowe Akademii Morskiej w Szczecinie* 62(134), pp. 108–115, doi: 10.17402/425.
19. QIAO, D., YAN, J. & OU, J. (2014) Effects of mooring line with buoys system on the global responses of a semi-submersible platform. *Brodogradnja* 65 (1), pp. 79–96.
20. ROBERTSON, A., JONKMAN, J., MASCIOLA, M., SONG, H., GOUPEE, A., COULLING, A. & LUAN, C. (2014) Definition of the Semisubmersible Floating System for Phase II of OC4. Technical Report, NREL/TP-5000-60601, National Renewable Energy Laboratory, U.S. Department of Energy. Available from: <https://www.nrel.gov/docs/fy14osti/60601.pdf>.
21. SABZIYAN, H., GHASSEMI, H., AZARSINA, F. & KAZEMI, S. (2014) Effect of Mooring Lines Pattern in a Semi-submersible Platform at Surge and Sway Movements. *Journal of Ocean Research* 2 (1), pp. 17–22, doi: 10.12691/jor-2-1-4.
22. SHOKOUHIAN, M., HEAD, M., SEO, J., SCHAFFER, W. & ADAMS, G. (2019) Hydrodynamic response of a semi-submersible platform to support a wind turbine. *Journal of Marine Engineering & Technology* 20 (3), pp. 170–185, doi: 10.1080/20464177.2019.1571662.
23. TAHAR, A. & KIM, M.H. (2008) Coupled-dynamic analysis of floating structures with polyester mooring lines. *Ocean Engineering* 35, pp. 1676–1685, doi: 10.1016/j.oceaneng.2008.09.004.
24. TANG, Y.-G., ZHANG, S.-X., ZHANG, R.-Y. & LIU, H.-X. (2007) Development of study on the dynamic characteristics of deep water mooring system. *Journal of Marine Science and Application* 6(3), pp. 17–23, doi:10.1007/s11804-007-7016-2.
25. VAN DEN BOOM, H.J.J. (1985) *Dynamic behaviour of mooring lines*. BOSS Conference, Delft, The Netherlands.
26. WANG, D. (2007) Static analysis of a wire rope-chain-buoy/sinker mooring line. *China Offshore Platform* 6, pp. 16–20.
27. YU, J., HAO, S., YU, Y., CHEN, B., CHENG, S. & WU, J. (2019) Mooring analysis for a whole TLP with TTRs under tendon one-time failure and progressive failure. *Ocean Engineering* 182, pp. 360–385, doi: 10.1016/j.oceaneng.2019.04.049.
28. YUAN, Z.-M., INCECIK, A. & Ji, C. (2014) Numerical study on a hybrid mooring system with clump weights and buoys. *Ocean Engineering* 88, pp. 1–11, doi: 10.1016/j.oceaneng.2014.06.002.

Cite as: Motallebi, M., Ghassemi, H., Shokouhian, M. (2022) DeepCwind semi-submersible floating offshore wind turbine platform with a nonlinear multi-segment catenary mooring line and intermediate buoy. *Scientific Journals of the Maritime University of Szczecin, Zeszyty Naukowe Akademii Morskiej w Szczecinie* 69 (141), 20–34.